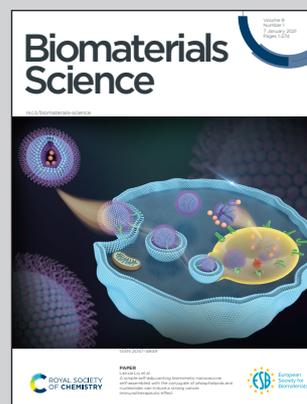Showcasing the research from the Engineered Microenvironments and Mechanobiology Lab in the Department of Biomedical Engineering at the University of Michigan.

Microenvironmental determinants of organized iPSC-cardiomyocyte tissues on synthetic fibrous matrices

This work demonstrates the importance of recapitulating the fibrous architecture and mechanics of myocardial ECM to engineer structurally organized iPSC-derived cardiomyocyte tissues using orthogonally tunable synthetic matrices.

As featured in:

Biomaterials Science

See Brendon M. Baker *et al.*, *Biomater. Sci.*, 2021, **9**, 93.

ROYAL SOCIETY OF CHEMISTRY

rsc.li/biomaterials-science

Registered charity number: 207890

PAPER

Check for updates

Microenvironmental determinants of organized iPSC-cardiomyocyte tissues on synthetic fibrous matrices†

Samuel J. DePalma, [a] Christopher D. Davidson, [a] Austin E. Stis,[a] Adam S. Helms[b] and Brendon M. Baker ⋆[a]

Cardiomyocytes derived from induced pluripotent stem cells (iPSC-CMs) show great potential for engineering myocardium to study cardiac disease and create regenerative therapies. However, iPSC-CMs typically possess a late embryonic stage phenotype, with cells failing to exhibit markers of mature adult tissue. This is due in part to insufficient knowledge and control of microenvironmental cues required to facilitate the organization and maturation of iPSC-CMs. Here, we employed a cell-adhesive, mechanically tunable synthetic fibrous extracellular matrix (ECM) consisting of electrospun dextran vinyl sulfone (DVS) fibers and examined how biochemical, architectural, and mechanical properties of the ECM impact iPSC-CM tissue assembly and subsequent function. Exploring a multidimensional parameter space spanning cell-adhesive ligand, seeding density, fiber alignment, and stiffness, we found that fibronectin-functionalized DVS matrices composed of highly aligned fibers with low stiffness optimally promoted the organization of functional iPSC-CM tissues. Tissues generated on these matrices demonstrated improved calcium handling and increased end-to-end localization of N-cadherin as compared to micropatterned fibronectin lines or fibronectin-coated glass. Furthermore, DVS matrices supported long-term culture (45 days) of iPSC-CMs; N-cadherin end-to-end localization and connexin43 expression both increased as a function of time in culture. In sum, these findings demonstrate the importance of recapitulating the fibrous myocardial ECM in engineering structurally organized and functional iPSC-CM tissues.

Introduction

Heart disease is the leading cause of death worldwide.[1] This is in part due to the fact that many cardiomyopathies lead to permanent damage to the myocardium, which has limited potential to regenerate. Existing therapies fail to restore cardiac function after damage arising from chronic conditions or traumatic injury from myocardial infarction.[2] Thus, there is a pressing need to develop engineered myocardial tissue that can be used in replacement or regenerative therapies. Additionally, physiologically representative *in vitro* models of cardiac tissue can aid in the advancement of our understanding of cardiac disease progression and the identification and subsequent development of effective pharmacologic interventions.

Cardiomyocytes derived from induced pluripotent stem cells (iPSC-CMs) show promise for engineering myocardium

for regenerative therapies and for disease modeling.[3] In recent years, there have been many advances in culture protocols to improve the efficiency of stem cell differentiation towards a myocardial lineage.[4–7] However, in most cases, iPSC-CM maturation stops at the late embryonic stage, with cells failing to exhibit hallmarks of maturity such as myofibril alignment, end-to-end polarization of gap junctions, and enhanced calcium handling.[3,8] More recent studies have demonstrated the ability to achieve higher levels of engineered cardiac tissue maturation through the use of naturally derived biomaterials (*e.g.* collagen, fibrin, and Matrigel) combined with iPSC-CMs and stromal cells, such as fibroblasts or mesenchymal stem cells.[4,9,10] Despite their success in improving the function of engineered cardiac tissues, the incorporation of stromal cell populations can confound study interpretation due to uncontrolled and uncharacterized crosstalk between these stromal support cells and cardiomyocytes (CMs). Therefore, there remains a need to engineer materials that can accurately present the appropriate physical and mechanical cues present in the native ECM to promote myocyte tissue formation in the absence of supporting cells.

The mechanical function of the myocardium is dictated by contractile CMs and the fibrous ECM that surrounds, orients,

[a]Department of Biomedical Engineering, University of Michigan, Ann Arbor, MI 48109, USA. E-mail: bambren@umich.edu
[b]Division of Cardiovascular Medicine, University of Michigan, Ann Arbor, MI 48109, USA

and groups them.[11] This complex, hierarchical collagen network organizes myocardium at multiple length scales: (1) epimysial collagen fibers surround large groups of muscle bundles to provide mechanical stability preventing excessive stretching of the tissue; (2) perimysial fibers wrap around and organize individual bundles of CMs; (3) small endomysial fibers found within each bundle connect to the cytoskeleton of each CM *via* costameres.[11–13] In particular, perimysial collagen fibers are approximately 1 μm in diameter and are co-aligned along the long axis of each CM bundle.[14] The structural organization of surrounding perimysial fiber networks parallel that of the myofibers within each muscle bundle. Together, highly aligned CMs and surrounding ECM enable mechanically anisotropic contractions critical to healthy cardiac function. The importance of this structure–function relationship is particularly evident in disease states such as fibrosis where fibroblasts deposit excessive amounts of disorganized matrix in the perimysial space, impairing overall tissue function.[11,15,16]

As it is evident that organized fibrous ECM plays a critical role in facilitating myofibrillar alignment, a number of material platforms have been developed to recapitulate these cell-instructive cues to drive structural and functional maturation of engineered cardiac tissue. ECM proteins can be micropatterned into anisotropic geometries (*e.g.* lines or rectangles) to organize attached CMs and improve tissue functionality.[17–19] However, these substrates lack cell-scale topographical cues reminiscent of perimysial matrix which may be required for myocardial tissue assembly and function. Attempts to better recapitulate cardiac ECM topography have included culturing iPSC-CMs on nanogrooved substrates.[20,21] While these methods promote robust structural alignment and higher tissue maturity, they lack mechanical tunability and fail to accurately mimic the complex fibrous topography cells experience *in vivo*. Electrospun scaffolds come closest to recapitulating perimysial network architecture, but commonly used electrospun biomaterials (*e.g.* polycaprolactone, polylactide-*co*-glycolide, or polyvinyl alcohol) are typically orders of magnitude stiffer than CMs or cardiac ECM.[5,22–27] This is particularly important given recent evidence that culture substrates with elastic moduli approximating that of native myocardium can enhance myofibril formation and overall tissue maturity.[17,28–31] Despite the success of these and other culture platforms in improving iPSC-CM tissue function, each of these approaches only mimic certain aspects of the cardiac ECM. As such, a comprehensive, multiparameter understanding of the physical environmental cues necessary to form high-functioning CM tissues is currently lacking. Thus, new biomaterial approaches are needed that can accurately and orthogonally recapitulate fibrous, biochemical, and mechanical attributes of the cardiac ECM to promote further maturation.

We previously developed a synthetic fibrous ECM-like material composed of polymeric fibers with comparable geometry to perimysial collagen fibers.[32] These fibers have a highly tunable elasticity over a range reflecting measurements of type I collagen fibers and enable user-defined control over

presented adhesive ligands and overall architectural organization. In this work, we alter biochemical, architectural, and mechanical properties of these synthetic fibrous matrices to identify critical ECM determinants to iPSC-CM attachment and subsequent tissue assembly, structure, and function. Systematically exploring a multidimensional biomaterial parameter space, we find that soft, aligned dextran vinyl sulfone (DVS) networks presenting fibronectin (FN) promote the highest levels of structural organization and function as assessed by calcium flux imaging. Additionally, we compare iPSC-CMs cultured in our material system to commonly used CM culture platforms that lack anisotropic adhesive cues or topography and find that compliant and aligned fibrous ECM yields the highest degree of iPSC-CM tissue organization and function. Lastly, we demonstrate the ability of DVS fiber matrices to facilitate long-term culture of iPSC-CMs that enables further structural organization as evidenced by end-to-end localization of cell–cell adhesions. Taken together, these studies highlight the importance of recapitulating key physical attributes of the cardiac extracellular microenvironment and isolating their respective influences on iPSC-CM tissues formation and maturation.

Experimental

Reagents

All reagents were purchased from Sigma Aldrich and used as received, unless otherwise stated.

DVS fibrous matrix fabrication

DVS polymer was synthesized as previously described by our lab.[32] Briefly, dextran was reacted with divinyl sulfone and the product was dialyzed and lyophilized. For electrospinning, DVS was dissolved at 0.7 g mL^{-1} in a 1 : 1 mixture of Milli-Q water and dimethylformamide with 0.6% (w/v) lithium phenyl-2,4,6-trimethylbenzoylphosphinate (LAP; Colorado Photopolymer Solutions) photoinitiator, 2.5% (v/v) methacrylated rhodamine (25 mM; Polysciences, Inc., Warrington, PA), and 5.0% (v/v) glycidyl methacrylate. This solution was electrospun on coverslips affixed to a custom-built rotating mandrel with a hexagonal geometry (Fig. 1a) driven by an AC motor with controllable speed. Electrospinning was conducted in an environmental chamber at 35% humidity with a flow rate of 0.2 ml h^{-1}, voltage of 7.0 kV, and a gap distance of ∼5 cm to the grounded mandrel. After collection, fibers were stabilized by primary crosslinking under UV (100 mW cm^{-2}) for 20 s, then hydrated in varying concentrations of LAP photoinitiator solution and exposed again to UV for 20 s to tune fiber stiffness. To functionalize matrices with FN or collagen (Corning International), 2.5% (w/v) heparin methacrylate (HepMA) was dissolved in LAP solution during secondary UV exposure. ECM proteins were diluted at a concentration of 50 μg mL^{-1} and adsorbed to fibers at RT for 1 hour. Alternatively, matrices were functionalized with cell adhesive peptides cyclized [Arg-Gly-Asp-ᴅ-Phe-Lys(Cys)] (cRGD; Peptides
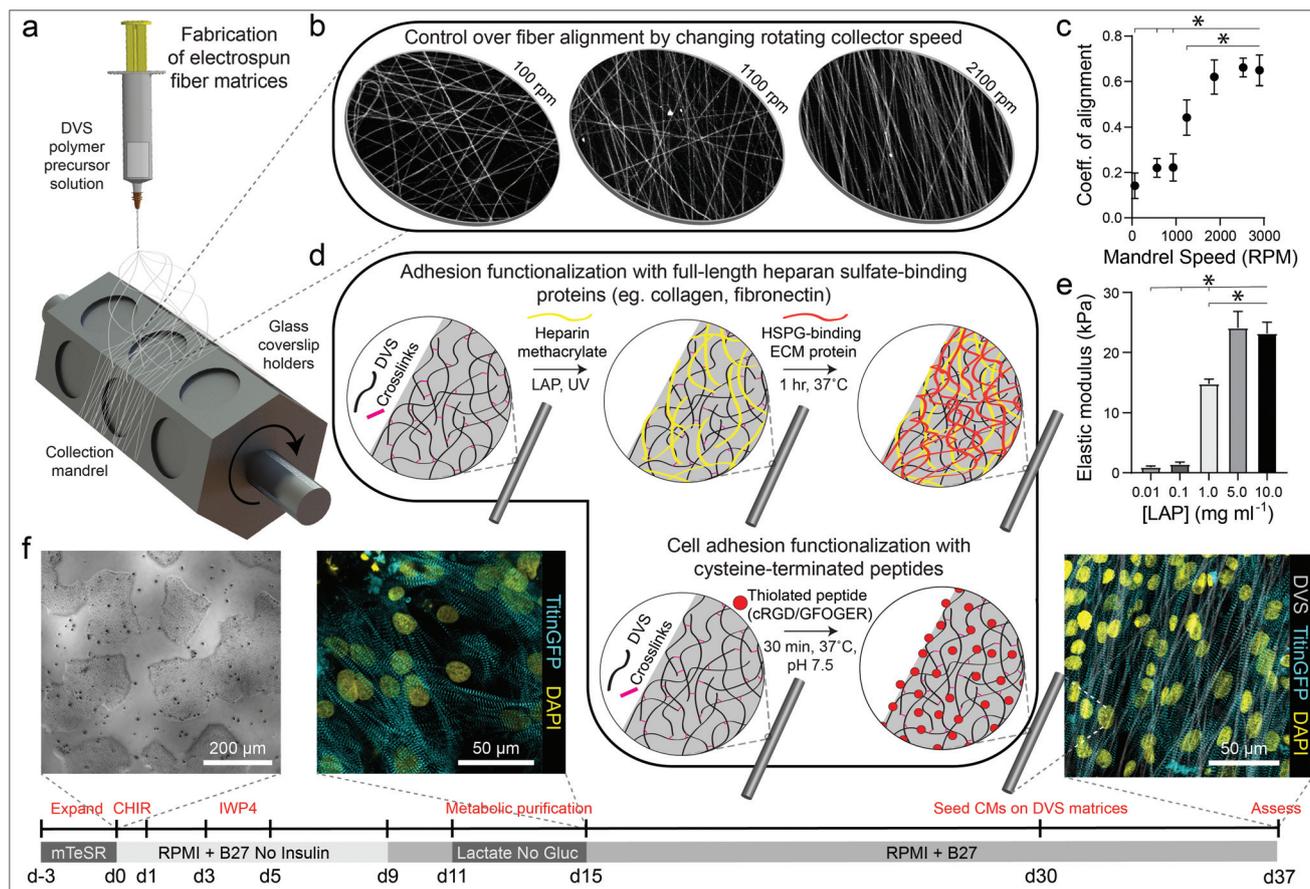
Fig. 1 Tunable DVS fibrous matrices for culturing iPSC-CMs. (a) Schematic of fabrication setup used to generate DVS matrices. A photocrosslinkable DVS polymer solution was electrospun and collected on glass coverslips affixed to a rotating hexagonal mandrel. (b and c) Mandrel rotation speed was varied to define fiber alignment. (d) To facilitate cell adhesion, fibers were functionalized with full length proteins fibronectin or collagen *via* a heparin sulfate conjugation scheme, or short adhesive peptides cRGD or GFOGER *via* Michael-type addition chemistry. (e) Fiber stiffness was tuned by altering the amount of photoinitiated crosslinking. (f) iPSCs were differentiated through temporal modulation of the Wnt signaling pathway as previously described,[38] purified *via* metabolic selection for at least 4 days, and seeded on DVS fibrous substrates 30 days post initiation of differentiation. Progression of the differentiation process can be seen from brightfield images of iPSCs taken before differentiating, immunofluorescent images of iPSC-CMs just after metabolic selection, and iPSC-CMs seeded on aligned DVS matrices. All data presented as mean ± std; $n \geq 5$ matrices; * $p < 0.05$.

International) or Gly-Phe-Hyp-Gly-Glu-Arg (GFOGER; CPC Scientific) *via* Michael-Type addition to available vinyl sulfone groups. Peptides were dissolved at 200 μM in Milli-Q water containing HEPES (50 mM), phenol red (10 μg mL⁻¹), and 1 M NaOH to bring the pH to 8.0. A volume of 150 μL was added to each substrate and incubated at room temperature for 30 min. Substrates were sterilized in 70% ethanol prior to cell seeding.

DVS matrix mechanical testing

Mechanical properties of DVS matrices were determined using previously developed methods.[32,33] Briefly, suspended networks of DVS were indented with a rigid SU8 cylinder affixed to a pure tungsten filament using a commercial CellScale Microsquisher (CellScale). Young's modulus was approximated assuming the material behaves as an elastic membrane as previously described.[32,33]

Microcontact printing

To create substrates to compare with DVS matrices, 3 μm wide FN parallel lines spaced 3 μm apart were created *via* traditional microcontact printing approaches. Using photolithography techniques, patterns were transferred to a silicon wafer spin-coated with 1 μm thickness Microposit S1813 photoresist (MicroChem). Following development, polydimethylsiloxane (PDMS) (Sylgard 184, Dow Corning) was cast on to wafers and cured at 80 °C for 2 h to generate micropatterned stamps. To visualize patterns, FN was fluorescently tagged with AlexaFluor555 succidinyl ester following the manufacturer's protocol. Briefly, a 1 mg mL⁻¹ solution of FN was reacted with AlexaFluor55 succidinyl ester at a 9-fold molar excess for 2 h at RT with agitation in a 1 M sodium bicarbonate solution and purified by dialysis (6.5 kDa cutoff). For microcontact printing, fluorescent FN was diluted to 50 μg mL⁻¹ in sterile Milli-Q water and adsorbed to the micropatterned stamps for 30 min

at RT. The fibronectin pattern was transferred to UV ozone activated, PDMS coated coverslips (*via* spin coating, 5000 rpm). After sitting overnight to allow for the recovery of hydrophobicity, substrates were sterilized in 70% ethanol and then incubated in Pluronics F-127 (0.2% w/v in Milli-Q water) for 30 min at RT to prevent protein and cell adhesion to non-printed regions of the substrate. To create control non-micropatterned substrates, FN (50 μg mL^{-1}) was adsorbed to UV ozone treated glass coverslips for >30 min at RT.

iPSC culture and CM differentiation

Induced pluripotent stem cells containing a GFP-titin reporter[34] (gift from the Seidman Lab) were cultured in mTeSR1 media (StemCell Technologies) and differentiated in RPMI 1640 media supplemented with B27 minus insulin (ThermoFisher). Differentiation was initiated on day 0 with the addition of 12 μM CHIR99021 for 24 hours and then 5 μM IWP4 on day 3 for 48 hours. On day 9, media insulin was introduced and cells began to contract on day 10. For CM purification, cultures were transferred to RPMI lacking glucose and glutamine (Biological Industries) supplemented with 4 mM DL-lactate on day 11 for 4–6 days. Following purification, CMs were maintained in CM maintenance media (RPMI 1640 supplemented with 2% (v/v) B27 (Thermo Fischer)). On day 30, CMs were dissociated using accutase (Corning) and seeded on fibrous matrices or control substrates. Cultures were maintained in CM maintenance media replenished every other day for the duration of studies. All studies were carried out for 7 days unless otherwise specified.

Calcium imaging

Calcium handling analysis was performed by incubating cells for 1 hour at 37 °C with 5 μM Cal520, AM (AAT Bioquest). Cells were then returned to conditioned media preserved prior to adding the calcium sensitive dye and allowed to equilibrate for >30 minutes at 37 °C and 5% CO_2. Following equilibration, tissues were imaged under epifluorescence at 96 Hz while maintaining temperature and CO_2.

Immunofluorescence staining

Samples were fixed in 2% paraformaldehyde for 15 min at RT. Autoflourescence quenching was performed by incubating samples in 0.1 M NH_4Cl (pH 8.0) for 10 min at RT, and then in a fresh NH_4Cl solution for an additional 5 min. This was followed by antigen retreival *via* incubation in pre-warmed 10 mM trisodium citrate dihydrate (pH 6.0) for 15 minutes. Samples were then permeablized in PBS solution containing Triton X-100 (0.2% v/v), sucrose (10% w/v), and magnesium chloride (0.6% w/v) for 10 min and blocked in 1% (w/v) bovine serum albumin. Tissues were incubated with mouse monoclonal anti-N-cadherin (1:200; BD Bioscience 610921) overnight at 4 °C, rabbit monoclonal anti-connexin43 (1:1000; Millipore Sigma AB1728) antibodies overnight at 4 °C, mouse monoclonal anti-α-actinin (1:500; Abcam ab9465) for 1 hour at RT, mouse monoclonal anti-cardiac troponin T (1:500; ThermoFisher MA5-12960) for 1 hour at RT, mouse mono-

clonal or rabbit monoclonal anti-Ki67 (1:1000; Sigma-Aldrich PIMA514520) for 1 hour at RT, followed by either goat anti-mouse Alex Fluor 647 (1:1000; Life Technologies A21236) or goat anti-rabbit Alexa Fluor 647 secondary antibodies, (1:1000; Life Technologies A21245) and DAPI for 1 hour at RT.

Image analysis

Time-lapse movies of calcium flux were analyzed with custom MATLAB scripts (Fig. S1†). Briefly, average fluorescent profiles over time were determined from select areas of each tissue and parameters such as beats per minute, peak-to-peak irregularity, flux rise time, flux decay time, and peak full width half max were calculated. Contraction correlation coefficient was determined by dividing the entire field of view into 16 regions of equal area and calculating the average Pearson's correlation coefficient between the flux profiles of each of these regions.[35] Sarcomere alignment was also quantified *via* custom MATLAB scripts (Fig. S2†). Briefly, images of titin-GFP reporter were thresholded and individual z-discs segmented. Z-discs were subsequently grouped with neighboring z-discs based on proximity and orientation to identify myofibrils within the image. The orientation of all identified myofibrils within a field of view was fit to a Gaussian distribution. Sarcomere alignment deviation was defined at the standard deviation of this distribution using circular/angular statistics.[36]

Statistical analysis

Statistical significance was determined by one-way analysis of variance (ANOVA) with *post-hoc* analysis (Tukey test), with significance indicated by $p < 0.05$. Studies were conducted a minimum of 3 times with at least $n = 3$ tissues per condition and the data presented are representative data sets from one these replicate studies. Specific sample size is indicated within corresponding figure legends and all data are presented as mean ± standard deviation.

Results and Discussion

Synthetic extracellular matrix fabrication and iPSC-CM seeding parameters

To mimic perimysial collagen networks of native myocardium, we fabricated fibrous matrices composed of electrospun DVS fibers following methods established in our lab.[32] We previously used this material system to investigate the effects of physical matrix properties on cell behaviors including fibroblast spreading and myofibroblast differentiation.[32,37] These studies demonstrated the mechanical tunability, biocompatibility, and stability of this material over long-term culture thus motivating its use as a suitable platform for studying iPSC-CM engineered tissue formation. Here, we altered biochemical, architectural, and mechanical parameters to examine how each feature impacts the structure and function of iPSC-CM tissues. Controlling the speed of a rotating, hexagonal mandrel with affixed glass coverslips reproducibly defined the degree of fiber alignment within each matrix

(Fig. 1a–c). Control over subsequent photoinitiated free radical polymerization *via* LAP photoinitiator concentration defined the degree of crosslinking within each fiber and resulting stiffness of bulk matrices (Fig. 1e). To facilitate cell attachment, fibers were functionalized with short cell-adhesive peptides cRGD or GFOGER directly coupled to remaining VS groups *via* Michael type addition. Alternatively, HepMA was covalently coupled to remaining VS groups to enable functionalization with full length heparin sulfate proteoglycan (HSPG)-binding ECM proteins, including collagen and fibronectin (Fig. 1d). iPSC-derived CMs were differentiated and purified as previously described,[38–40] then seeded on substrates of varying material parameters and subsequently characterized by immunostaining and calcium imaging (Fig. 1f). Differentiation of iPSC-CMs was further confirmed by immunofluorescent staining of α-actinin and cardiac troponin T (Fig. S3†). In contrast to electrospun materials that have been previously used to induce cardiac tissue organization and function, DVS matrices provide concurrent and orthogonal architectural, mechanical, and biochemical control, enabling careful dissection of how iPSC-CMs respond to critical ECM features known to vary with the age and disease status of cardiac tissue.[16,41–43]

Having defined parameters to control biochemical and biophysical attributes of DVS matrices, we next sought to identify adhesive ligands that facilitate robust iPSC-CM attachment to aligned DVS fiber matrices, given previous observations that anisotropic substrates promote the formation of organized cardiac tissues.[5,18,20,24] Matrices were functionalized for cell adhesion with full length ECM proteins type I collagen or fibronectin, or shorter peptides containing their integrin-binding domains, GFOGER or cRGD, respectively. Fiber diameter remained consistant regardless of functionalization scheme (Fig. S4a†). Overall, there was less robust iPSC-CM adhesion on substrates modified with GFOGER or full length type I collagen as compared to cRGD or fibronectin (Fig. 2a and b). In general, engineered healthy myocardium exhibits regular and synchronous patterns of calcium flux as well as highly aligned contractile machinery, as aberrations to these characteristics have been implicated in a number of disease states, including cardiac fibrosis.[16,35] Therefore, the overall functionality of iPSC-CM tissues was assessed by live imaging with a calcium sensitive dye after an additional 7 days of culture on engineered substrates. The spontaneous beat rate of tissues was found to be consistent across adhesive moieties (Fig. 2c). We found that tissues cultured on matrices presenting cRGD or fibronectin contract with a more regular frequency and more synchronously across the tissue surface (Fig. 2d and e; Fig. S1; Movie S1†). These findings are in line with the critical role of fibronectin in myocardial development
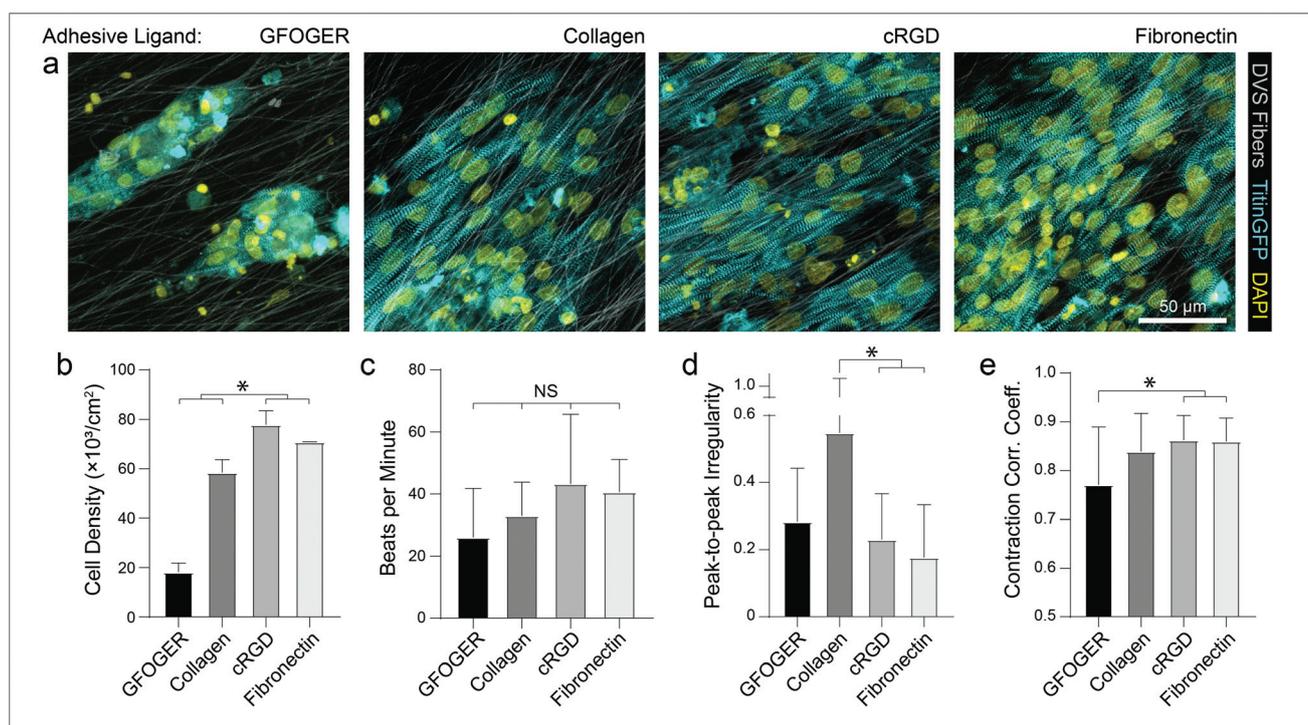

Fig. 2 DVS functionalization with FN and cRGD increase cell attachment and enable formation of contractile tissues. (a) Confocal fluorescent images of iPSC-CMs cultured on aligned DVS matrices functionalized with different cell-adhesive proteins or peptides. (b) Density of resultant iPSC-CM tissues on fibers functionalized with different cell adhesion functionalization schemes. Calcium flux dynamics were analyzed to determine (c) contraction rate, (d) peak-to-peak irregularity, as quantified by the standard deviation of time interval between peaks, and (e) contraction correlation coefficient for formed tissues, as calculated by Pearson's correlation coefficient between fluorescent profiles of subdivided regions within a field of view. All data presented as mean ± std; $n \geq 8$ fields of view across 3 tissues; * $p < 0.05$.

and in facilitating CM integrin engagement to the ECM *in vivo*.[44,45] Inhibition of the integrin α5 subunit, a receptor that predominately binds fibronectin, during cardiac development has demonstrated a critical role for this specific binding moiety in cardiac morphogenesis.[46,47] More recently, Neiman *et al.* highlighted the importance of the α5 subunit in iPSC differentiation to CMs *in vitro*, as knockdown of this integrin resulted in less efficient differentiation, suggesting that defined integrin binding could further dictate CM differention *in vitro*.[48] These results indicate that fibronectin or its cRGD derivative exhibit superior capacity for *in vitro* cardiac tissue generation on our fibrous matrices as compared to collagen. Although no functional differences in tissues created on fibronectin and cRGD functionalized matrices were noted, full-length fibronectin was utilized in all subsequent studies described below, given its importance in the cardiac ECM and widespread use in other iPSC-CM studies.[18,44,49,50] Previous work has also demonstrated the potential utility of functiona-

lizing ECM mimetic scaffolds with developmentally informed bioactive ligands to direct stem cell differentiation.[51–53] For example, Li *et al.* showed that coupling a Wnt5a mimetic ligand, Foxy5, to hyaluronic acid scaffolds increased noncanonical Wnt signaling, enhanced mechanotransduction through RhoA-ROCK signaling, and drove osteogenic differentiation of human mesenchymal stem cells.[52] In separate studies, cardiac tissue regeneration was improved post-infarction after the introduction of nanofibers functionalized with insulin-like growth factor 1.[53] Thus, the effect of presenting other bioactive ligands in addition to integrin-binding proteins or peptides is worth exploring in future work.

As different adhesive ligands resulted in variations in attachment and subsequent CM density that correlated with calcium transient synchronicity, we next sought to determine the optimal density of CMs required to create an organized and functional layer of tissue on fibronectin-functionalized DVS matrices (Fig. 3a). At low seeding densities (50 and
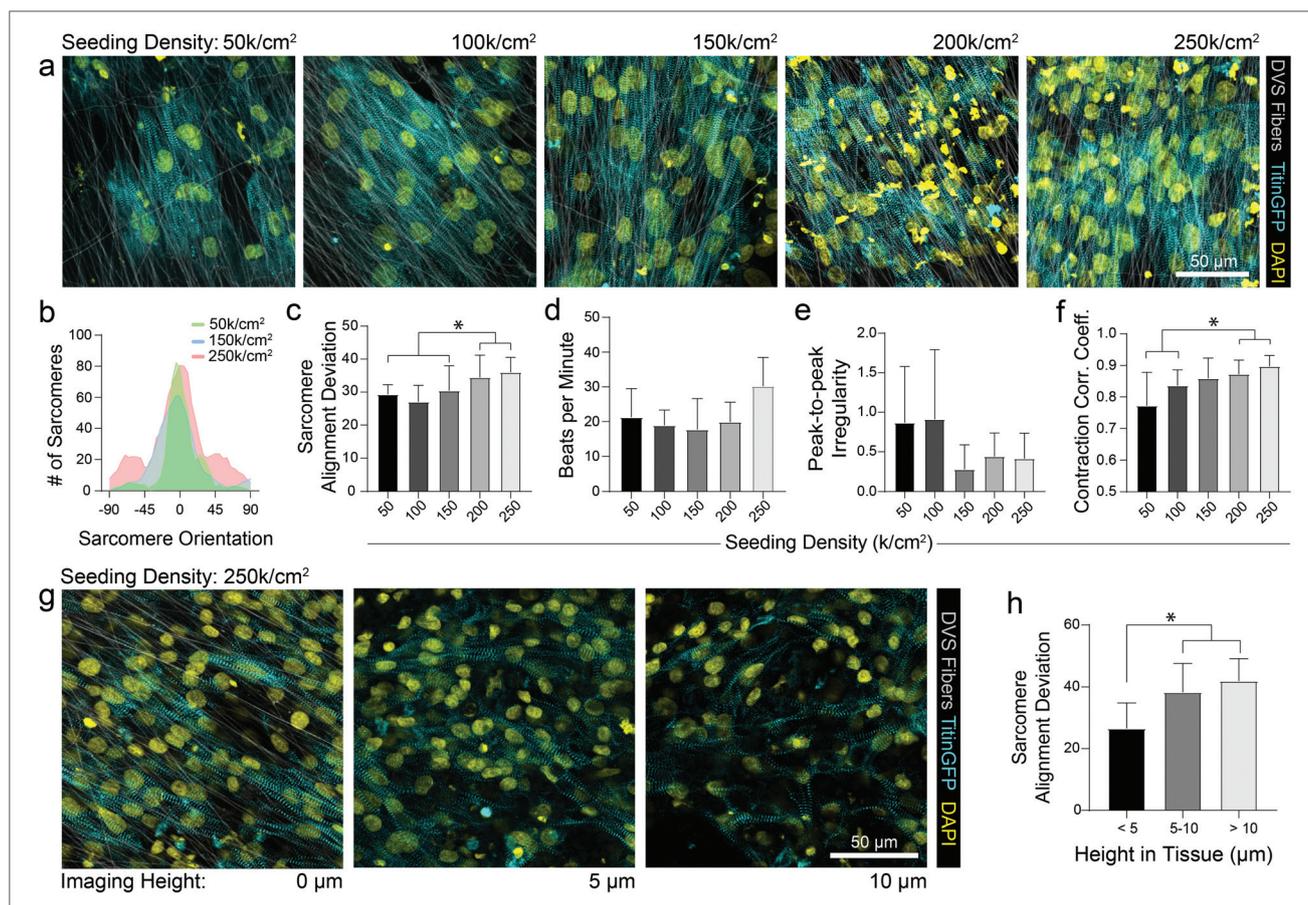

Fig. 3 iPSC-CMs at intermediate seeding density form highly organized and functional tissues. (a) Confocal fluorescent images of iPSC-CMs on aligned DVS matrices functionalized with fibronectin seeded at different densities ranging from 50 to 250k cm^{-2}. (b) Histogram of distribution of sarcomere angle in representative tissues seeded at 50, 150, and 250k cm^{-2}. (c) Quantification of overall sarcomere alignment of tissues seeded at densities ranging from 50 to 250k cm^{-2}. (d) Beat rate, (e) peak-to-peak irregularity and (f) contraction correlation coefficient for formed tissues obtained *via* analysis of calcium fluxes. (g) Image slices at 0, 5, and 10 μm from substrate surface taken *via* confocal microscopy within a dense (250k cm^{-2}) tissue. (h) Sarcomere alignment deviation of slices within specified height ranges for tissues seeded at 250k cm^{-2}. All data presented as mean ± std; $n \geq 8$ fields of view across 3 tissues; * $p < 0.05$.

100k cm^{-2}), myofibrils in resulting tissues were highly aligned, as quantified by image analysis of titinGFP-demarcated sarcomeres (Fig. S2†), however confluent monolayers did not form across the matrix (Fig. 3a–c). Disconnections across the monolayer resulted in greater beat irregularity and lower synchronicity across the tissue (Fig. 3e and f; Movie S2†). At higher seeding densities (200 and 250k cm^{-2}), beat rates were more consistent and synchronous, but an increase in the angular deviation of myofibrils was noted (Fig. 3a–f; Movie S2†). Optical sectioning through the thickness of tissues by confocal microscopy revealed that cells directly in contact with the underlying matrix possessed highly aligned myofibrils (Fig. 3g and h). iPSC-CMs farther away from the matrix surface were increasingly disorganized as evidenced by an increase in myofibril angular deviation (Fig. 3g and h). These results highlight the significant role that ECM architecture plays in iPSC-CM organization.[11,14] Given these findings, an intermediate seeding density (150k cm^{-2}) was selected for subsequent studies. This seeding density yields a confluent layer of iPSC-CMs where all cells receive alignment cues from the underlying matrix. CM density has also been shown to affect overall tissue function in other previously established *in vitro* models.[9] Shadrin *et al.* found that iPSC-CMs in a 3D hydrogel at high densities had reduced force output per cell and increased conduction velocity, most likely due to restricted space for CMs to grow in these dense tissues.[9] These findings further motivate the use of intermediate seeding densities on DVS where iPSC-CMs are given adequate space to spread as they sense the fibrous matrix below.

Effect of altered matrix alignment and mechanics on iPSC-CMs

The preceding studies imply that contact with aligned fibrous matrices is critical for creating iPSC-CM tissues with organized myofibrils. To confirm that matrix architecture dictates tissue organization, we next examined how alterations to the alignment of the fibrous matrices affect iPSC-CM tissue organization and function. As previously described, fiber alignment can be easily defined by changing the speed of the rotating collector (Fig. 1c). Seeding iPSC-CMs on nonaligned (100 rpm; 0.916 m s^{-1}), intermediate (1100 rpm; 10.1 m s^{-1}), and aligned (2100 rpm; 19.3 m s^{-1}) matrices resulted in increasing levels of myofibril organization (Fig. 4a and b). Matrix alignment also resulted in increased synchronicity across the tissue but no change in peak-to-peak irregularity (Fig. 4c and d; Movie S3†). Furthermore, tissues formed on nonaligned matrices exhibited longer calcium flux rise and decay times (Fig. 4e), both of which are established indicators of immaturity in tissues.[4,9] This finding is consistent with other studies indicating the importance of matrix anisotropy in generating cardiac tissues with enhanced organization and calcium handling.[5,18,20,24] Interestingly, the data presented here suggests that while the highest degree of fiber alignment induced greater myofibril alignment (Fig. 4b), an intermediate degree of fiber alignment was sufficient for rapid calcium handling (Fig. 4c–e). Previous studies have shown that integrin organization and overall
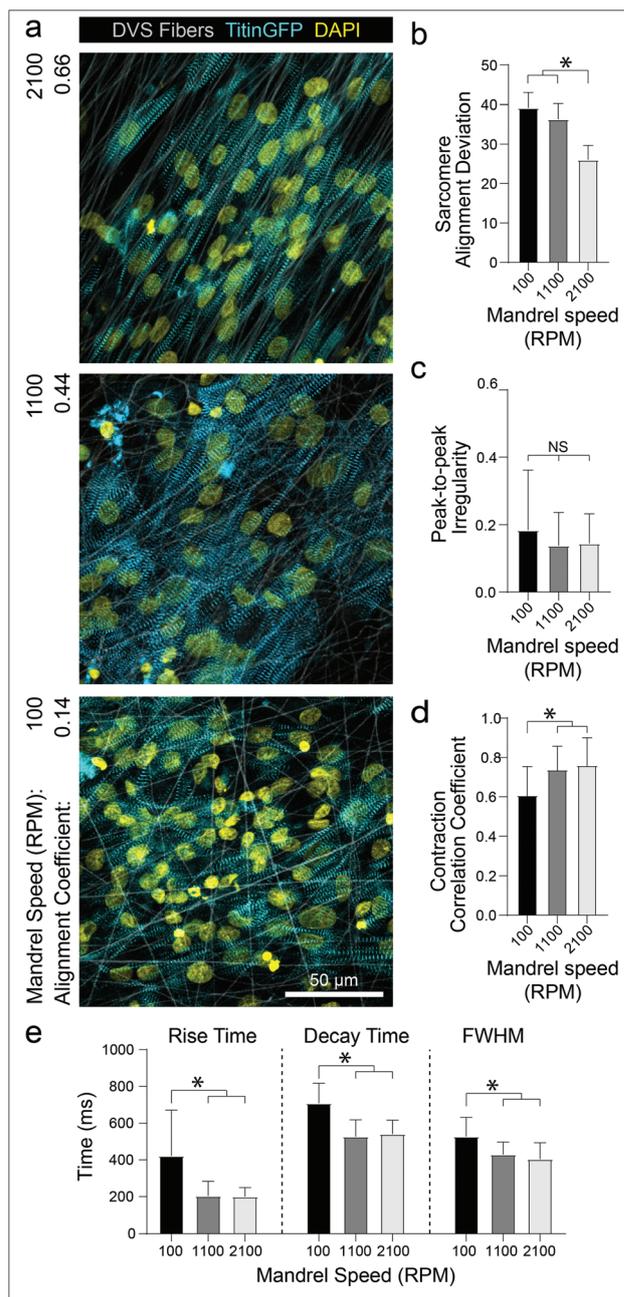

Fig. 4 Aligned matrices promote myofibril organization and improve tissue function. (a) Confocal fluorescent images of iPSC-CMs seeded on aligned (2100 rpm), intermediate (1100 rpm), and random (100 rpm). (b) Quantification of sarcomere alignment deviation. (c) Peak-to-peak and (d) correlation coefficient irregularity, as calculated from calcium flux data. (e) Individual calcium fluxes were analyzed to determine flux rise time, decay time, and peak full width half max. All data presented as mean $\pm$ std; $n \geq 12$ fields of view across 3 tissues; * $p < 0.05$.

structural anisotropy directly influences the organization and expression of calcium handling machinery within cardiomyocytes, leading to changes in overall tissue function.[3,17,50] These data suggest however that only an intermediate degree of adhesive or topographical anisotropy is necessary to elicit

improvements in calcium handling. As fine control over matrix alignment is straightforward with this platform, future studies could explore how matrix alignment guides subcellular organization in the contexts of cardiac development, during which the ECM transitions from disorganized to highly ordered between gestation days 100 and 143,[41] or disease progression, characterized by increasing deposition of disorganized matrix.[11,16]

In conjunction with organizational cues, substrate stiffness close to that of healthy cardiac tissues has also been shown to promote further functional maturation of CMs compared to culture on tissue culture plastic or glass.[17,28–30] For example, Ribeiro *et al.* showed that culturing CMs on non-fibrous hydrogel substrates approximating the stiffness of myocardium (~10 kPa) resulted in higher functioning CMs, whereas stiffer substrates hindered structural, functional, and transcriptional development of iPSC-CMs.[17] These findings have been corroborated by studies using other hydrogel systems,[29–31] but these settings fail to recapitulate the fibrous architecture of native cardiac ECM. Additionally, electrospun fibrous materials used to induce greater iPSC-CM function are typically supraphysiologic in stiffness and lack mechanical tunability.[5,22,24] After defining matrix architecture, DVS matrix stiffness can be tuned over the range of Young's moduli reported for developmental (<6 kPa), physiologic (9–14 kPa), and pathophysiologic myocardial tissues (>20 kPa)[31] *via* tuning photocrosslinking (Fig. 1d).[32]

To examine if iPSC-CMs sense changes to the stiffness of fibrous matrices, we controlled the amount of photoinitiated crosslinking of the DVS fibers while keeping matrix fiber density and alignment constant.[32] Altering the stiffness of the underlying fibers had no effect on myofibril alignment or beat synchronicity (Fig. 5a, b and d). However, iPSC-CMs cultured on low stiffness fibers (~1 kPa) resulted in greater calcium flux regularity with faster calcium fluxes in contrast to tissues generated on stiffer fibers (>20 kPa) (Fig. 5c and e; Movie S4†). These findings indicate that CMs can sense the stiffness of the matrix despite the fact that fibers were tethered to an underlying rigid glass surface that did not support fractional shortening of contracting tissues. This mechanoresponse may potentially be modulated by non-muscle myosin activity at costameres or integrin clustering, both of which have been previously shown to activate structural and functional changes in CMs.[50,54,55] There was also evidence of cell force-mediated matrix deformations and permanent reorganization on soft fiber matrices, as indicated by lateral translocations of fibers; in contrast, no deformations were evident in matrices of stiffer fibers (Fig. S5†). Additionally, as it has been suggested that CM proliferation can increase on stiffer substrates,[56] we examined iPSC-CM proliferation after 7 days of culture by immunostaining for Ki67, a proliferation marker. We find that iPSC-CMs on DVS matrices exhibited low proliferation rates with no differences noted across the range of stiffnesses explored here (Fig. S6†).

We next explored how simultaneously altering matrix architecture and mechanics influenced iPSC-CM-matrix inter-
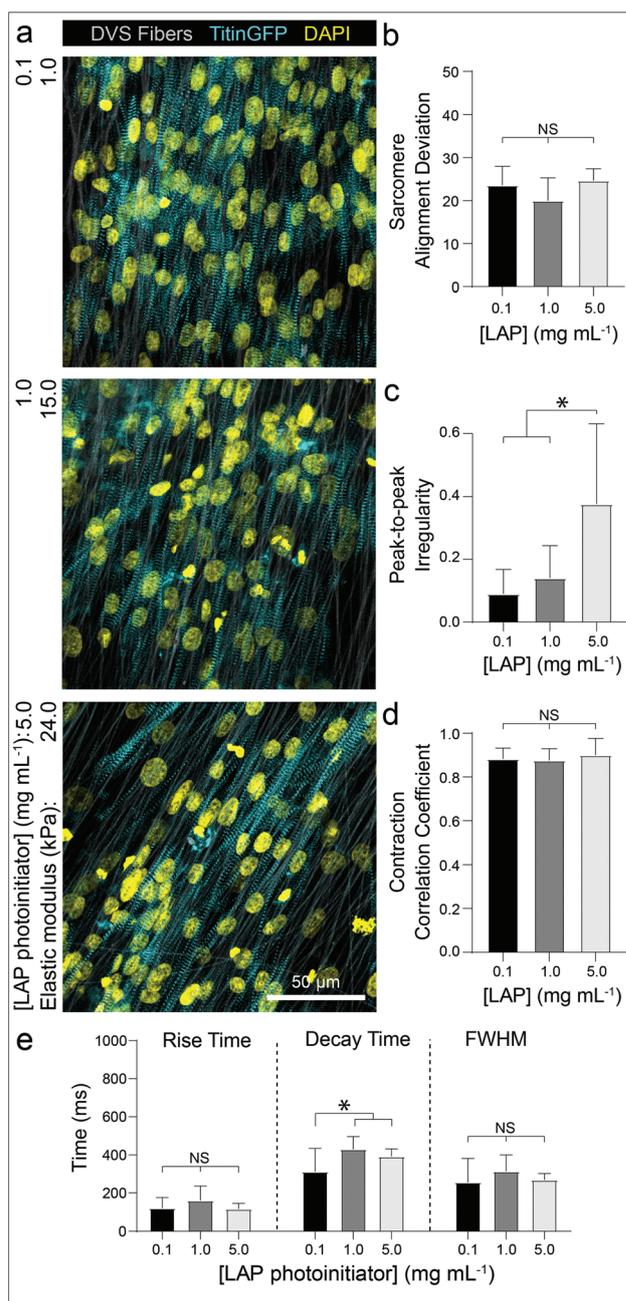

Fig. 5 iPSC-CMs on soft, DVS fibers exhibit improved calcium handling. (a) Confocal fluorescent images of iPSC-CMs seeded on aligned matrices composed of DVS fibers of differing stiffnesses by tuning photoinitiated crosslinking *via* photoinitiator (LAP) concentration. (b) Quantification of sarcomere alignment deviation. (c) Correlation coefficient and (d) peak-to-peak irregularity, as calculated from calcium flux data. (e) Individual calcium fluxes were analyzed to determine flux rise time, decay time, and peak full width half max. All data presented as mean ± std; $n \geq 12$ fields of view across 3 tissues; * $p < 0.05$.

actions. iPSC-CMs were seeded on DVS matrices with orthogonally varied alignment and stiffness and immunostained for the focal adhesion (FA) protein, vinculin. Custom image analysis was used to segment and quantify the total FA area per

cell, the average size of individual FAs within each cell, and the aspect ratio of adhesions (Fig. S7a†). While the alignment of matrix fibers increased the aspect ratio and size of individual FAs (Fig. S7c and d†), total FA area per cell appeared to be affected by both fiber organization and stiffness, with soft/non-aligned fibers expressing similar overall FA area to both soft/aligned and stiff/aligned matrices (Fig. S7b†). Softer matrices may lead to increased FA adhesion formation *via* the increased nanoscale flexibility of adhesive ligands, thereby enabling integrin clustering required for focal adhesion formation.[32,57–59] Additionally, we qualitatively noted an impact on the organization of FAs which aligned with their long axis in the direction of myofibrils and underlying DVS fibers. On aligned matrices, FAs appeared to co-localize with sarcomeres, potentially to optimally mechanically support the more organized contractile myofibrils within aligned iPSC-CMs. The influence of fiber alignment on iPSC-CM myofibril assembly and organization may explain the equivalent total FAs area per cell of stiff/aligned matrices as compared to soft/aligned or soft/nonaligned matrices.[19] This potential additive effect is reiterated by the marked increase in FA aspect ratio on soft aligned matrices as compared to all other matrix conditions (Fig. S7d†). These results highlight the importance of orthogonally controlling fiber organization and mechanics when studying how CMs respond to changes in their microenvironment.

DVS matrices afford improved tissue organization and function over other platforms

While ECM-coated tissue culture plastic or glass remain a typical setting for studies of iPSC-CMs, the use of micropatterned or topographical substrates to promote tissue organization and improve overall function has become increasingly common.[5,17,18,20,22,24] To explore the relative importance of anisotropic adhesive patterning *vs.* topographical cues, we compared tissue organization and calcium handling characteristics of iPSC-CMs cultured on fibronectin-functionalized DVS matrices, microcontact-printed fibronectin lines, and fibronectin adsorbed to glass substrates (Fig. 6). Soft aligned DexVS matrices were selected for this comparison, as they guided the formation of the highest functioning tissues in the studies above. Microcontact-printed arrays of fibronectin lines (3 μm width with 3 μm spacing) on glass were chosen to approximate the adhesive surface area and alignment of DVS fibers and non-patterned fibronectin-coated glass served as a control. Functionally, iPSC-CMs seeded on DVS matrices exhibited more regular and synchronous calcium transients compared to tissues on micropatterned and non-patterned fibronectin (Fig. 6b and c; Movie S5†). Furthermore, DVS induced faster rise and decay times in calcium fluxes (Fig. 6d). Structurally, iPSC-CMs on DVS matrices exhibited the highest levels of myofibrillar organization (Fig. 6a and b). As the native myocardium matures, proteins such as N-cadherin and connexin43 localize end-to-end at intercalated discs to enable directional propagation of action potentials.[60] Immunostaining for N-cadherin, we noted more frequent end-to-end localization on DVS

matrices than on glass controls or micropatterned lines where such localization was not observed (Fig. 6a). Although the mechanism mediating this localization requires further study, this observation suggests a critical requirement for both topography and anisotropic adhesive cues afforded by fibers.

Long term culture of iPSC-CMs on DVS matrices

In addition to these improvements in subcellular organization quantified after 7 days in culture, DVS matrices also supported long-term culture of iPSC-CMs. Whereas confluent iPSC-CMs seeded on both micropatterned and non-patterned fibronectin detached from underlying substrates after 8–10 days of culture due to their innate contractile forces, DVS matrices enabled culture of purified confluent iPSC-CMs to at least 45 days post-seeding (Fig. 6f). High magnification imaging of tissues immunostained for vinculin demonstrated increased numbers of costameres distributed at greater density across multiple imaging planes in DVS matrices compared to standard substrates (Fig. S8†). This suggests that the three-dimensional nature of DVS fibers promotes increased cell-ECM adhesion to stabilize tissues. Long-term culture of iPSC-CM on fibrous matrices could facilitate time-dependent maturation processes required for intercalated disc assembly or T-tubule formation.[3] A number of other studies have also applied external mechanical or electrical stimuli to drive maturation of tissues.[4,61–63] Given the long-term stability of these tissues and the facile deposition of DVS fibers on elastomer or electrically conductive substrates, future studies will explore these important maturation signals.

Previous work has shown that long-term culture (up to 45 days) of non-confluent iPSC-CM facilitates further maturation, as characterized by improved sarcomere organization, hypertrophy, reduced proliferation, and enhanced calcium handling.[3,64] As we observed improved iPSC-CM subcellular organization and function after 7 days on DVS matrices, we hypothesized that prolonged culture of pure, confluent iPSC-CMs could facilitate further maturation. Culturing iPSC-CMs on soft, aligned DexVS matrices for up to 28 days, we observed no changes in calcium handling outputs including rise and decay time as a function of culture duration (Fig. 7e–g). End-to-end localization of N-cadherin to intercellular junctions was evident at all time points while myofibril alignment remained constant (Fig. 7a and b). Since connexin43 accumulates in developing gap junctions during development, we also stained for this protein in tissues on aligned DVS matrices.[60,65] Immunostaining for connexin43 revealed increased production as a function of culture duration, further indicating that anisotropic fibrous cues drive the assembly of key subcellular structures (Fig. 7c and d; Fig. S9†). Changes in connexin43 localization and other maturation markers over time warrants further study, and in sum we conclude that while structural cues guide tissue organization and function, they alone are not sufficient for driving significant iPSC-CM tissue maturity.

Previous studies have also suggested limitations to long-term culture on substrates that solely define tissue anisotropy,
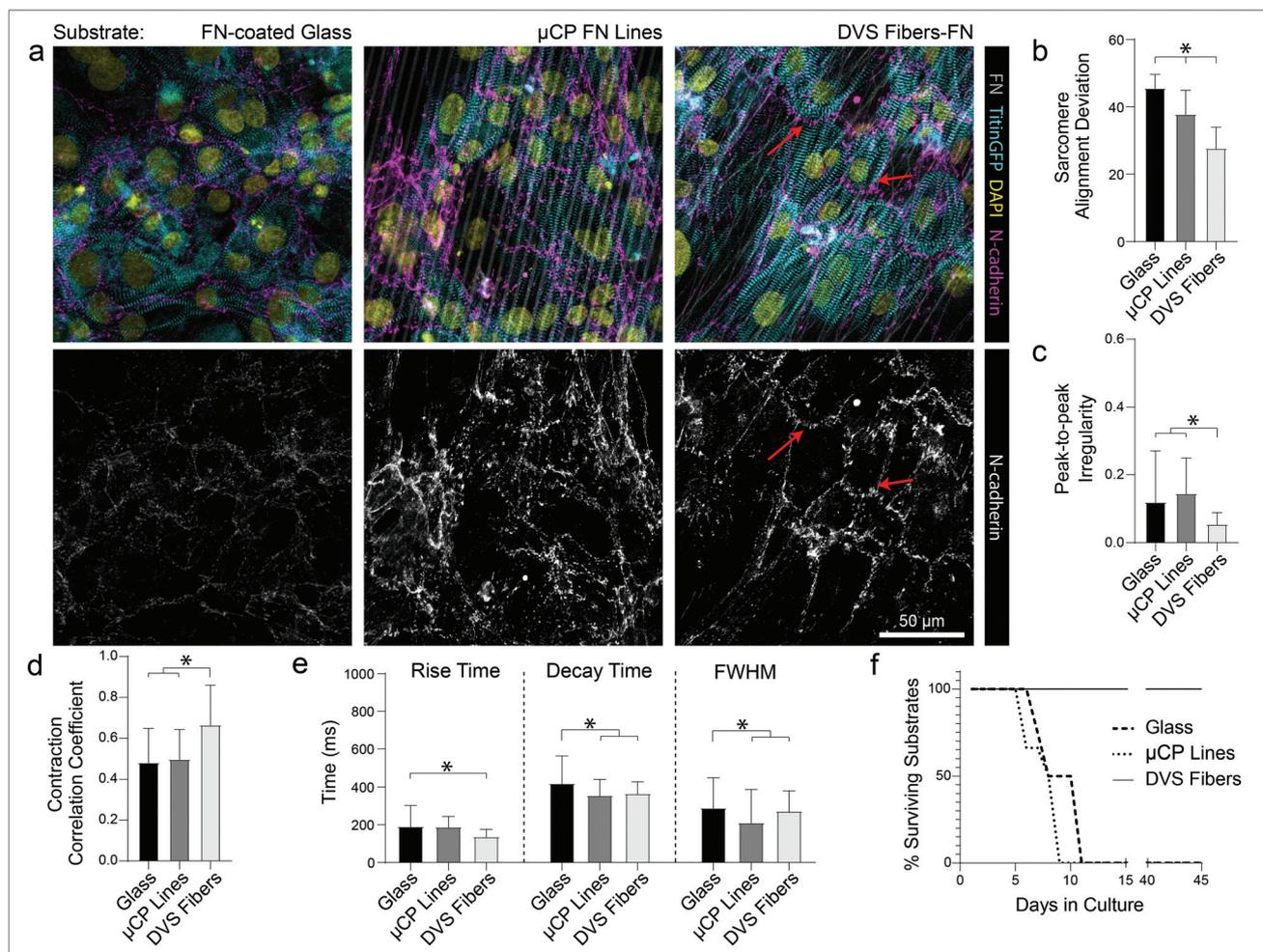
Fig. 6 Fibrous DVS matrices promote increased tissue function and organization and allow for long-term culture of confluent iPSC-CMs. (a) Confocal fluorescent images of iPSC-CMs seeded on fibronectin-coated glass, microcontact printed fibronectin lines, and aligned DVS fibers modified with adhesive fibronectin after 7 days in culture. Red arrows indicate areas of N-cadherin localization at end-end cell junctions. (b) Quantification of sarcomere angle deviation across all substrates. (c) Calcium handling quantifications of peak-to-peak irregularity, (d) contraction correlation coefficient, and (e) flux rise time, decay time, and full width half max. (f) Survival of cultures over time on various substrates. All data presented as mean $\pm$ std; $n \geq 12$ fields of view across 3 tissues; * $p < 0.05$.

indicating that while alignment cues induce the expression of some maturation markers, further maturation requires the addition of other stimuli such as mechanical loading, electrical pacing, soluble factors or even other heterotypic cell communication with supporting cell types.[3,4,6,7,10,63,66] Nevertheless, organizational cues provided by DVS matrices that mimic aspects of the native perimysial ECM appear to drive cardiac tissue assembly and function by controlling adhesive signaling between iPSC-CMs and the ECM. Despite this, DVS matrices fail to recapitulate the more complex hierarchical organization of the cardiac ECM, limiting the study of how cues from other ECM layers, and interactions between them, impact overall tissue function.[11] By altering electrospinning parameters, fibrous matrices could be fabricated with fiber diameters and mechanics similar to epimysial and endomysial networks.[22] The future development of scalable technologies to generate tissues from multiple layers of

iPSC-CM-laden fibrous matrices could provide a route to regenerative or tissue replacement therapies.[67]

In addition, mechanosensing of ECM properties by CMs has been shown to be vital during cardiac tissue development and in supporting healthy tissue function, but many studies, including the ones described here, indicate that this relationship requires further investigation.[3,43,68] Other work in our lab has explored the influence of fiber mechanics on cell spreading, migration, and multicellular network assembly by suspending matrices over microfabricated wells in contrast to the studies described above depositing fibers on rigid coverslips.[32,33,69] As both passive and active mechanical properties of the ECM have been shown to foster tissue maturation,[17,29,62,70,71] exploration of the iPSC-CMs response to ECM settings that enable fractional shortening of tissues is a focus of ongoing investigations. Studies such as these could provide further insights into how CMs respond to dynamic
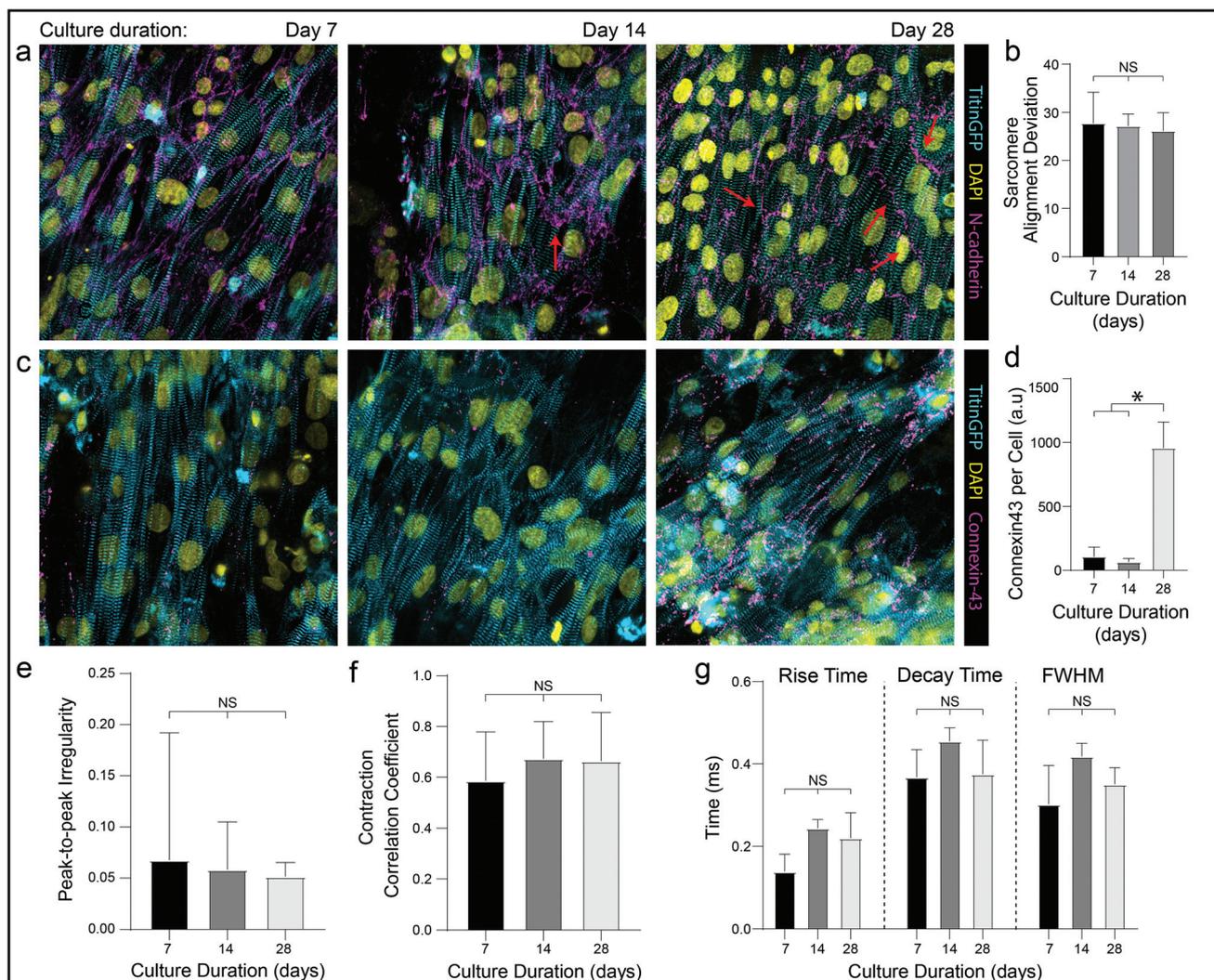
Fig. 7 Aligned fibrous matrices induce myofibril organization and improve tissue function. Confocal fluorescent images of iPSC-CMs seeded on DVS cultured for 7, 14, and 28 days with immunostaining for (a) N-cadherin and (c) connexin43. Red arrows indicate localization of N-cadherin at end-to-end cell–cell junctions. (b) Quantification of sarcomere angle deviation over time. (d) Quantification of connexin43 expression over time. (e) Calcium handling quantifications of peak-to-peak irregularity, (f) contraction correlation coefficient, and (g) flux rise time, decay time, and full width half max. All data presented as mean $\pm$ std; $n \geq 12$ fields of view across 3 tissues; * $p < 0.05$.

mechanical changes of the ECM and could be integrated with previously established pacing protocols to promote iPSC-CM maturation.

Conclusion

In summary, we established synthetic, tunable DVS fibrous matrices that model perimysial collagen networks of native myocardium. Varying adhesive ligand, architecture, and mechanics of these matrices, we found that soft, aligned DVS fibers functionalized with fibronectin or cRGD best facilitate the formation of organized and contractile iPSC-CM tissue layers. Fibrous topographical cues and anisotropic distribution of adhesive ligand improved calcium handling, enhanced structural organization, including N-cadherin end-to-end localiz-

ation, and enabled long-term culture of iPSC-CM tissues. While our results support the notion that fibrous ECM cues are not sufficient in generating iPSC-CM tissues with adult-like phenotypes, prolonged culture on DVS matrices promoted N-cadherin end-to-end localization and increased connexin43 expression. Taken together, these studies motivate the inclusion of fibrous cues in biomaterial culture platforms towards generating mature iPSC-CM tissues for applications in replacement/regenerative therapies, disease modeling, and drug screening.

Conflicts of interest

The authors have no conflicts of interest to declare.

Acknowledgements

References

1 S. S. Virani, A. Alonso, E. J. Benjamin, M. S. Bittencourt, C. W. Callaway, A. P. Carson, A. M. Chamberlain, A. R. Chang, S. Cheng, F. N. Delling, L. Djousse, M. S. V. Elkind, J. F. Ferguson, M. Fornage, S. S. Khan, B. M. Kissela, K. L. Knutson, T. W. Kwan, D. T. Lackland, T. T. Lewis, J. H. Lichtman, C. T. Longenecker, M. S. Loop, P. L. Lutsey, S. S. Martin, K. Matsushita, A. E. Moran, M. E. Mussolino, A. M. Perak, W. D. Rosamond, G. A. Roth, U. K. A. Sampson, G. M. Satou, E. B. Schroeder, S. H. Shah, C. M. Shay, N. L. Spartano, A. Stokes, D. L. Tirschwell, L. B. VanWagner and C. W. Tsao, Heart Disease and Stroke Statistics—2020 Update: A Report From the American Heart Association, *Circulation*, 2020, **141**, e139–e596.

2 S. Funakoshi, K. Miki, T. Takaki, C. Okubo, T. Hatani, K. Chonabayashi, M. Nishikawa, I. Takei, A. Oishi, M. Narita, M. Hoshijima, T. Kimura, S. Yamanaka and Y. Yoshida, Enhanced engraftment, proliferation, and therapeutic potential in heart using optimized human iPSC-derived cardiomyocytes, *Sci. Rep.*, 2016, **6**, 1–14.

3 E. Karbassi, A. Fenix, S. Marchiano, N. Muraoka, K. Nakamura, X. Yang and C. E. Murry, *Nat. Rev. Cardiol.*, 2020, **17**, 341–359.

4 K. Ronaldson-Bouchard, S. P. Ma, K. Yeager, T. Chen, L. J. Song, D. Sirabella, K. Morikawa, D. Teles, M. Yazawa and G. Vunjak-Novakovic, Advanced maturation of human cardiac tissue grown from pluripotent stem cells, *Nature*, 2018, **556**, 239–243.

5 A. C. B. Allen, E. Barone, N. Momtahan, C. O. Crosby, C. Tu, W. Deng, K. Polansky and J. Zoldan, Temporal Impact of Substrate Anisotropy on Differentiating Cardiomyocyte Alignment and Functionality, *Tissue Eng., Part A*, 2019, **25**, 1426–1437.

6 X. Yang, M. L. Rodriguez, A. Leonard, L. Sun, K. A. Fischer, Y. Wang, J. Ritterhoff, L. Zhao, S. C. Kolwicz, L. Pabon, H. Reinecke, N. J. Sniadecki, R. Tian, H. Ruohola-Baker, H. Xu and C. E. Murry, Fatty Acids Enhance the Maturation of Cardiomyocytes Derived from Human Pluripotent Stem Cells, *Stem Cell Rep.*, 2019, **13**, 657–668.

7 J. C. Garbern, A. Helman, R. Sereda, M. Sarikhani, A. Ahmed, G. O. Escalante, R. Ogurlu, S. L. Kim, J. F. Zimmerman, A. Cho, L. MacQueen, V. J. Bezzerides, K. K. Parker, D. A. Melton and R. T. Lee, Inhibition of mTOR Signaling Enhances Maturation of Cardiomyocytes Derived From Human-Induced Pluripotent Stem Cells via p53-Induced Quiescence, *Circulation*, 2020, **141**, 285–300.

8 H. Uosaki, P. Cahan, D. I. Lee, S. Wang, M. Miyamoto, L. Fernandez, D. A. Kass and C. Kwon, Transcriptional Landscape of Cardiomyocyte Maturation, *Cell Rep.*, 2015, **13**, 1705–1716.

9 I. Y. Shadrin, B. W. Allen, Y. Qian, C. P. Jackman, A. L. Carlson, M. E. Juhas and N. Bursac, Cardiopatch platform enables maturation and scale-up of human pluripotent stem cell-derived engineered heart tissues, *Nat. Commun.*, 2017, **8**, 1825.

10 E. Giacomelli, V. Meraviglia, G. Campostrini, A. Cochrane, X. Cao, R. W. J. van Helden, A. Krotenberg Garcia, M. Mircea, S. Kostidis, R. P. Davis, B. J. van Meer, C. R. Jost, A. J. Koster, H. Mei, D. G. Míguez, A. A. Mulder, M. Ledesma-Terrón, G. Pompilio, L. Sala, D. C. F. Salvatori, R. C. Slieker, E. Sommariva, A. A. F. de Vries, M. Giera, S. Semrau, L. G. J. Tertoolen, V. V. Orlova, M. Bellin and C. L. Mummery, Human-iPSC-Derived Cardiac Stromal Cells Enhance Maturation in 3D Cardiac Microtissues and Reveal Non-cardiomyocyte Contributions to Heart Disease, *Cell Stem Cell*, 2020, **26**, 799–801.

11 K. T. Weber, Cardiac interstitium in health and disease: The fibrillar collagen network, *J. Am. Coll. Cardiol.*, 1989, **13**, 1637–1652.

12 K. T. Weber, Y. Sun, S. C. Tyagi and J. P. M. Cleutjens, *J. Mol. Cell. Cardiol.*, 1994, **26**, 279–292.

13 S. Fleischer and T. Dvir, Tissue engineering on the nano-scale: Lessons from the heart, *Curr. Opin. Biotechnol.*, 2013, **24**, 664–671.

14 A. J. Pope, G. B. Sands, B. H. Smaill and I. J. LeGrice, Three-dimensional transmural organization of perimysial collagen in the heart, *Am. J. Physiol.: Heart Circ. Physiol.*, 2008, **295**, 1243–1252.

15 M. D. Davidson, J. A. Burdick and R. G. Wells, Engineered Biomaterial Platforms to Study Fibrosis, *Adv. Healthcare Mater.*, 2020, 1901682.

16 P. Kong, P. Christia and N. G. Frangogiannis, *Cell. Mol. Life Sci.*, 2014, **71**, 549–574.

17 A. J. S. Ribeiro, Y.-S. Ang, J.-D. Fu, R. N. Rivas, T. M. A. Mohamed, G. C. Higgs, D. Srivastava and B. L. Pruitt, Contractility of single cardiomyocytes differentiated from pluripotent stem cells depends on physiological shape and substrate stiffness, *Proc. Natl. Acad. Sci. U. S. A.*, 2015, **112**, 12705–12710.

18 S. P. Sheehy, A. Grosberg, P. Qin, D. J. Behm, J. P. Ferrier, M. A. Eagleson, A. P. Nesmith, D. Krull, J. G. Falls, P. H. Campbell, M. L. McCain, R. N. Willette, E. Hu and K. K. Parker, Toward improved myocardial maturity in an organ-on-chip platform with immature cardiac myocytes, *Exp. Biol. Med.*, 2017, **242**, 1643–1656.

19 M. L. McCain, H. Lee, Y. Aratyn-Schaus, A. G. Kléber and K. K. Parker, Cooperative coupling of cell-matrix and cell-cell adhesions in cardiac muscle, *Proc. Natl. Acad. Sci. U. S. A.*, 2012, **109**, 9881–9886.

20 D. Carson, M. Hnilova, X. Yang, C. L. Nemeth, J. H. Tsui, A. S. T. Smith, A. Jiao, M. Regnier, C. E. Murry, C. Tamerler and D. H. Kim, *ACS Appl. Mater. Interfaces*, 2016, **8**, 21923–21932.

21 J. I. Luna, J. Ciriza, M. E. Garcia-Ojeda, M. Kong, A. Herren, D. K. Lieu, R. A. Li, C. C. Fowlkes, M. Khine and K. E. McCloskey, Multiscale biomimetic topography for the alignment of neonatal and embryonic stem cell-derived heart cells, *Tissue Eng., Part C*, 2011, **17**, 579–588.

22 S. Fleischer, J. Miller, H. Hurowitz, A. Shapira and T. Dvir, Effect of fiber diameter on the assembly of functional 3D cardiac patches, *Nanotechnology*, 2015, **26**, 1–10.

23 J. Yu, A.-R. Lee, W.-H. Lin, C.-W. Lin, Y.-K. Wu and W.-B. Tsai, Electrospun PLGA Fibers Incorporated with Functionalized Biomolecules for Cardiac Tissue Engineering, *Tissue Eng., Part A*, 2014, **20**, 1896–1907.

24 M. Wanjare, L. Hou, K. H. Nakayama, J. J. Kim, N. P. Mezak, O. J. Abilez, E. Tzatzalos, J. C. Wu and N. F. Huang, Anisotropic microfibrous scaffolds enhance the organization and function of cardiomyocytes derived from induced pluripotent stem cells, *Biomater. Sci.*, 2017, **5**, 1567–1578.

25 J. Li, I. Minami, M. Shiozaki, L. Yu, S. Yajima, S. Miyagawa, Y. Shiba, N. Morone, S. Fukushima, M. Yoshioka, S. Li, J. Qiao, X. Li, L. Wang, H. Kotera, N. Nakatsuji, Y. Sawa, Y. Chen and L. Liu, Human Pluripotent Stem Cell-Derived Cardiac Tissue-like Constructs for Repairing the Infarcted Myocardium, *Stem Cell Rep.*, 2017, **9**, 1546–1559.

26 M. Khan, Y. Xu, S. Hua, J. Johnson, A. Belevych, P. M. L. Janssen, S. Gyorke, J. Guan and M. G. Angelos, Evaluation of Changes in Morphology and Function of Human Induced Pluripotent Stem Cell Derived Cardiomyocytes (HiPSC-CMs) Cultured on an Aligned-Nanofiber Cardiac Patch, *PLoS One*, 2015, **10**, e0126338.

27 M. Kharaziha, M. Nikkhah, S. R. Shin, N. Annabi, N. Masoumi, A. K. Gaharwar, G. Camci-Unal and A. Khademhosseini, PGS:Gelatin nanofibrous scaffolds with tunable mechanical and structural properties for engineering cardiac tissues, *Biomaterials*, 2013, **34**, 6355–6366.

28 T. J. Herron, A. M. Da Rocha, K. F. Campbell, D. Ponce-Balbuena, B. C. Willis, G. Guerrero-Serna, Q. Liu, M. Klos, H. Musa, M. Zarzoso, A. Bizy, J. Furness, J. Anumonwo, S. Mironov and J. Jalife, Extracellular matrix-mediated maturation of human pluripotent stem cell-derived cardiac monolayer structure and electrophysiological function, *Circ.: Arrhythmia Electrophysiol.*, 2016, **9**, e003638.

29 J. L. Young and A. J. Engler, Hydrogels with time-dependent material properties enhance cardiomyocyte differentiation in vitro, *Biomaterials*, 2011, **32**, 1002–1009.

30 J. G. Jacot, A. D. McCulloch and J. H. Omens, Substrate stiffness affects the functional maturation of neonatal rat ventricular myocytes, *Biophys. J.*, 2008, **95**, 3479–3487.

31 A. J. Engler, C. Carag-Krieger, C. P. Johnson, M. Raab, H. Y. Tang, D. W. Speicher, J. W. Sanger, J. M. Sanger and D. E. Discher, Embryonic cardiomyocytes beat best on a matrix with heart-like elasticity: Scar-like rigidity inhibits beating, *J. Cell Sci.*, 2008, **121**, 3794–3802.

32 C. D. Davidson, D. K. P. Jayco, D. L. Matera, S. J. DePalma, H. L. Hiraki, W. Y. Wang and B. M. Baker, Myofibroblast activation in synthetic fibrous matrices composed of dextran vinyl sulfone, *Acta Biomater.*, 2020, **105**, 78–86.

33 B. M. Baker, B. Trappmann, W. Y. Wang, M. S. Sakar, I. L. Kim, V. B. Shenoy, J. A. Burdick and C. S. Chen, Cell-mediated fibre recruitment drives extracellular matrix mechanosensing in engineered fibrillar microenvironments, *Nat. Mater.*, 2015, **14**, 1262–1268.

34 A. Sharma, C. N. Toepfer, T. Ward, L. Wasson, R. Agarwal, D. A. Conner, J. H. Hu and C. E. Seidman, CRISPR/Cas9-Mediated Fluorescent Tagging of Endogenous Proteins in Human Pluripotent Stem Cells, *Curr. Protoc. Hum. Genet.*, 2018, **96**, 21.11.1–21.11.20.

35 A. Kumar, S. K. Thomas, K. C. Wong, V. Lo Sardo, D. S. Cheah, Y. H. Hou, J. K. Placone, K. P. Tenerelli, W. C. Ferguson, A. Torkamani, E. J. Topol, K. K. Baldwin and A. J. Engler, Mechanical activation of noncoding-RNA-mediated regulation of disease-associated phenotypes in human cardiomyocytes, *Nat. Biomed. Eng.*, 2019, **3**, 137–146.

36 P. Berens, CircStat: A MATLAB Toolbox for Circular Statistics, *J. Stat. Softw.*, 2009, **31**, 1–21.

37 D. L. Matera, W. Y. Wang, M. R. Smith, A. Shikanov and B. M. Baker, Fiber Density Modulates Cell Spreading in 3D Interstitial Matrix Mimetics, *ACS Biomater. Sci. Eng.*, 2019, **5**, 2965–2975.

38 X. Lian, C. Hsiao, G. Wilson, K. Zhu, L. B. Hazeltine, S. M. Azarin, K. K. Raval, J. Zhang, T. J. Kamp and S. P. Palecek, Robust cardiomyocyte differentiation from human pluripotent stem cells via temporal modulation of canonical Wnt signaling, *Proc. Natl. Acad. Sci. U. S. A.*, 2012, **109**, E1848–E1857.

39 S. Tohyama, F. Hattori, M. Sano, T. Hishiki, Y. Nagahata, T. Matsuura, H. Hashimoto, T. Suzuki, H. Yamashita, Y. Satoh, T. Egashira, T. Seki, N. Muraoka, H. Yamakawa, Y. Ohgino, T. Tanaka, M. Yoichi, S. Yuasa, M. Murata, M. Suematsu and K. Fukuda, Distinct Metabolic Flow Enables Large-Scale Purification of Mouse and Human Pluripotent Stem Cell-Derived Cardiomyocytes, *Cell Stem Cell*, 2013, **12**, 127–137.

40 S. Tohyama, J. Fujita, T. Hishiki, T. Matsuura, F. Hattori, R. Ohno, H. Kanazawa, T. Seki, K. Nakajima, Y. Kishino, M. Okada, A. Hirano, T. Kuroda, S. Yasuda, Y. Sato, S. Yuasa, M. Sano, M. Suematsu and K. Fukuda, Glutamine Oxidation Is Indispensable for Survival of Human Pluripotent Stem Cells, *Cell Metab.*, 2016, **23**, 663–674.

41 C. Williams and L. D. Black, in *Biomaterials for Cardiac Regeneration*, Springer International Publishing, 2015, pp. 1–35.

42 R. J. Mccormick and D. P. Thomas, Collagen Crosslinking in the Heart: Relationship to Development and Function, *Basic Appl. Myol.*, 1998, **8**, 143–150.

43 J. G. Jacot, J. C. Martin and D. L. Hunt, Mechanobiology of cardiomyocyte development, *J. Biomech.*, 2010, **43**, 93–98.

44 F. Farhadian, F. Contard, A. Corbier, A. Barrieux, L. Rappaport and J. L. Samuel, Fibronectin expression during physiological and pathological cardiac growth, *J. Mol. Cell. Cardiol.*, 1995, **27**, 981–990.

45 M. Lockhart, E. Wirrig, A. Phelps and A. Wessels, *Birth Defects Res., Part A*, 2011, **91**, 535–550.

46 S. Israeli-Rosenberg, A. M. Manso, H. Okada and R. S. Ross, *Circ. Res.*, 2014, **114**, 572–586.

47 A. Mittal, M. Pulina, S. Y. Hou and S. Astrof, Fibronectin and integrin alpha 5 play requisite roles in cardiac morphogenesis, *Dev. Biol.*, 2013, **381**, 73–82.

48 G. Neiman, M. A. Scarafía, A. La Greca, N. L. Santín Velazque, X. Garate, A. Waisman, A. M. Möbbs, T. H. Kasai-Brunswick, F. Mesquita, D. Martire-Greco, L. N. Moro, C. Luzzani, A. Bastos Carvalho, G. E. Sevlever, A. Campos de Carvalho, A. S. Guberman and S. G. Miriuka, Integrin alpha-5 subunit is critical for the early stages of human pluripotent stem cell cardiac differentiation, *Sci. Rep.*, 2019, **9**, 1–10.

49 A. Chopra, M. L. Kutys, K. Zhang, W. J. Polacheck, C. C. Sheng, R. J. Luu, J. Eyckmans, J. T. Hinson, J. G. Seidman, C. E. Seidman and C. S. Chen, Force Generation via β-Cardiac Myosin, Titin, and α-Actinin Drives Cardiac Sarcomere Assembly from Cell-Matrix Adhesions, *Dev. Cell*, 2018, **44**, 87–96.

50 S. Sengupta, K. E. Rothenberg, H. Li, B. D. Hoffman and N. Bursac, Altering integrin engagement regulates membrane localization of Kir2.1 channels, *J. Cell Sci.*, 2019, **132**, jcs225383.

51 L. Bian, M. Guvendiren, R. L. Mauck and J. A. Burdick, Hydrogels that mimic developmentally relevant matrix and N-cadherin interactions enhance MSC chondrogenesis, *Proc. Natl. Acad. Sci. U. S. A.*, 2013, **110**, 10117–10122.

52 R. Li, S. Lin, M. Zhu, Y. Deng, X. Chen, K. Wei, J. Xu, G. Li and L. Bian, Synthetic presentation of noncanonical Wnt5a motif promotes mechanosensing-dependent differentiation of stem cells and regeneration, *Sci. Adv.*, 2019, **5**, 3896–3912.

53 M. E. Padin-Iruega, Y. Misao, M. E. Davis, V. F. M. Segers, G. Esposito, T. Tokunou, K. Urbanek, T. Hosoda, M. Rota, P. Anversa, A. Leri, R. T. Lee and J. Kajstura, Cardiac progenitor cells and biotinylated insulin-like growth factor-1 nanofibers improve endogenous and exogenous myocardial regeneration after infarction, *Circulation*, 2009, **120**, 876–887.

54 C. E. Chan and D. J. Odde, Traction dynamics of filopodia on compliant substrates, *Science*, 2008, **322**, 1687–1691.

55 P. Pandey, W. Hawkes, J. Hu, W. V. Megone, J. Gautrot, N. Anilkumar, M. Zhang, L. Hirvonen, S. Cox, E. Ehler, J. Hone, M. Sheetz and T. Iskratsch, Cardiomyocytes Sense Matrix Rigidity through a Combination of Muscle and Non-muscle Myosin Contractions, *Dev. Cell*, 2018, **44**, 326–336.

56 P. Bajaj, X. Tang, T. A. Saif and R. Bashir, Stiffness of the substrate influences the phenotype of embryonic chicken cardiac myocytes, *J. Biomed. Mater. Res., Part A*, 2010, **95A**, 1261–1269.

57 B. Trappmann, J. E. Gautrot, J. T. Connelly, D. G. T. Strange, Y. Li, M. L. Oyen, M. A. Cohen Stuart, H. Boehm, B. Li, V. Vogel, J. P. Spatz, F. M. Watt and W. T. S. Huck, Extracellular-matrix tethering regulates stem-cell fate, *Nat. Mater.*, 2012, **11**, 642–649.

58 B. T. Houseman and M. Mrksich, *The microenvironment of immobilized Arg-Gly-Asp peptides is an important determinant of cell adhesion*, 2001, vol. 22.

59 M. Arnold, E. A. Cavalcanti-Adam, R. Glass, J. Blümmel, W. Eck, M. Kantlehner, H. Kessler and J. P. Spatz, Activation of integrin function by nanopatterned adhesive interfaces, *ChemPhysChem*, 2004, **5**, 383–388.

60 A. Vreeker, L. van Stuijvenberg, T. J. Hund, P. J. Mohler, P. G. J. Nikkels and T. A. B. van Veen, Assembly of the Cardiac Intercalated Disk during Pre- and Postnatal Development of the Human Heart, *PLoS One*, 2014, **9**, e94722.

61 A. Mihic, J. Li, Y. Miyagi, M. Gagliardi, S. H. Li, J. Zu, R. D. Weisel, G. Keller and R. K. Li, The effect of cyclic stretch on maturation and 3D tissue formation of human embryonic stem cell-derived cardiomyocytes, *Biomaterials*, 2014, **35**, 2798–2808.

62 J. L. Ruan, N. L. Tulloch, M. Saiget, S. L. Paige, M. V. Razumova, M. Regnier, K. C. Tung, G. Keller, L. Pabon, H. Reinecke and C. E. Murry, Mechanical stress promotes maturation of human myocardium from pluripotent stem cell-derived progenitors, *Stem Cells*, 2015, **33**, 2148–2157.

63 J. L. Ruan, N. L. Tulloch, M. V. Razumova, M. Saiget, V. Muskheli, L. Pabon, H. Reinecke, M. Regnier and C. E. Murry, Mechanical Stress Conditioning and Electrical Stimulation Promote Contractility and Force Maturation of Induced Pluripotent Stem Cell-Derived Human Cardiac Tissue, *Circulation*, 2016, **134**, 1557–1567.

64 S. D. Lundy, W. Z. Zhu, M. Regnier and M. A. Laflamme, Structural and functional maturation of cardiomyocytes derived from human pluripotent stem cells, *Stem Cells Dev.*, 2013, **22**, 1991–2002.

65 G. I. Fishman, E. L. Hertzberg, D. C. Spray and L. A. Leinwand, Expression of connexin43 in the developing rat heart, *Circ. Res.*, 1991, **68**, 782–787.

66 J. Han, Q. Wu, Y. Xia, M. B. Wagner and C. Xu, Cell alignment induced by anisotropic electrospun fibrous scaffolds alone has limited effect on cardiomyocyte maturation, *Stem Cell Res.*, 2016, **16**, 740–750.

67 S. Fleischer, A. Shapira, R. Feiner and T. Dvir, Modular assembly of thick multifunctional cardiac patches, *Proc. Natl. Acad. Sci. U. S. A.*, 2017, **114**, 1898–1903.

68 K. K. Parker and D. E. Ingber, Extracellular matrix, mechanotransduction and structural hierarchies in heart tissue engineering, *Philos. Trans. R. Soc., B*, 2007, **362**, 1267–1279.

69 C. D. Davidson, W. Y. Wang, I. Zaimi, D. K. P. Jayco and B. M. Baker, Cell force-mediated matrix reorganization

underlies multicellular network assembly, *Sci. Rep.*, 2019, **9**, 12.

70 J. L. Young, K. Kretchmer, M. G. Ondeck, A. C. Zambon and A. J. Engler, Mechanosensitive kinases regulate stiffness-induced cardiomyocyte maturation, *Sci. Rep.*, 2014, **4**, 1–11.

71 A. Leonard, A. Bertero, J. D. Powers, K. M. Beussman, S. Bhandari, M. Regnier, C. E. Murry and N. J. Sniadecki, Afterload promotes maturation of human induced pluripotent stem cell derived cardiomyocytes in engineered heart tissues, *J. Mol. Cell. Cardiol.*, 2018, **118**, 147–158.